Anharmonic Franck−Condon Simulation of the Absorption and Fluorescence Spectra for the Low-Lying S_1 and S_2 Excited States of Pyridine†

Huan Wang,‡,§ Chaoyuan Zhu,*,‡ Jian-Guo Yu,*,§ and Sheng Hsien Lin‡

Department of Applied Chemistry, Institute of Molecular Science and Center for Interdisciplinary Molecular Science, National Chiao-Tung University, Hsinchu 30050, Taiwan, and Department of Chemistry, Beijing Normal University, Beijing 100875, P. R. China

Received: April 19, 2009; Revised Manuscript Received: May 22, 2009

Anharmonic effects of the absorption and fluorescence spectra of pyridine molecule are studied and analyzed for the two-low lying singlet excited states $S_1(^1B_1)$ and $S_2(^1B_2)$. The complete active space self-consistent field (CASSCF) method is utilized to compute equilibrium geometries and all 27 vibrational normal-mode frequencies for the ground state and the two excited states. The present calculations show that the frequency differences between the ground and two excited states are small for the ten totally symmetric vibrational modes so that the displaced oscillator approximation can be used for spectrum simulations. The Franck−Condon factors within harmonic approximation basically grasp the main features of molecular spectra, but simulated 0−0 transition energy position and spectrum band shapes are not satisfactorily good for $S_1(^1B_1)$ absorption and fluorescence spectra in comparison with experiment observation. As the first-order anharmonic correction added to Franck−Condon factors, both spectrum positions and band shapes can be simultaneously improved for both absorption and fluorescence spectra. It is concluded that the present anharmonic correction produces a significant dynamic shifts for spectrum positions and improves spectrum band shapes as well. The detailed structures of absorption spectrum of $S_2(^1B_2)$ state observed from experiment can be also reproduced with anharmonic Franck−Condon simulation, and these were not shown in the harmonic Franck−Condon simulation with either distorted or Duschinsky effects in the literature.

I. Introduction

Theoretical simulation of molecular dynamics and spectroscopy starts from Born−Oppenheimer approximation, within which electronically ground-state and excited-state wave functions are calculated with further approximation methods from conventional Ab. initio quantum chemistry. Within Born−Oppenheimer approximation, the Franck−Condon[1−3] (FC) overlap integrals of vibrational wave functions belonging to two different electronic states are essential quantities in the theoretical description for the vibronic structure of electronic spectra like UV absorption, fluorescence, and other nonradiative processes like electronic and energy transfer. Exact calculation for multidimensional FC overlap integrals is not practical for many-atom systems. Harmonic approximation with normal-mode analysis is commonly utilized to interpret experimental spectroscopy and anharmonic correction to harmonic approximation is sometime necessary for making improvement of simulation. Under harmonic and/or anharmonic approximation, further approximations can be classified regarding to difference between ground-state and excited-state vibrational normarl modes as displaced oscillator approximation, distorted oscillator approximation, and normal mode-mixing with including Duschinsky effect.[4] Various analytical and numerical methods are developed to compute FC overlap integrals with applications to molecular spectroscopy and energy and electron transfer processes.[5−35]

Pyridine molecule has been extensively studied by both experiments and theoretical simulations for its low-lying excited states with applications to photophysics and photochemistry. The lowest singlet excited state S_1 has symmetry and transition type of $^1B_1$ ($n\rightarrow\pi^*$) through experimental absorption spectrum[36] and also high resolution optothermal spectroscopy.[37] The fluorescence emission spectrum was also experimentally observed for S_1 state.[38] The second lowest singlet excited state S_2 has symmetry and transition type of $^1B_2$ ($\pi\rightarrow\pi^*$) through experimental absorption spectrum.[39] There are a large number of computational studies on equilibrium geometries, vibrational frequencies, and spectra for ground state and low-lying excited states of pyridine.[40−46] Franck−Condon simulations within displaced harmonic oscillator approximation including distorted effects were performed for S_1 and S_2 absorption spectra,[40] and simulations including Duschinsky effect were performed as well.[41] Both distorted and Duschinsky effects seem small for absorption spectra of pyridine. It is our motivation in the present studies to investigate anharmonic effects on the absorption and fluorescence spectra for pyridine, especially the first-order anharmonic approximation that is the leading contribution to spectra is actually performed. With analytical formulation of absorption and fluorescence coefficients[35] as well as computational formulas for the certain anharmonic constants,[47,48] we have a powerful tool to demonstrate a distinguished contribution, in which the shifts of spectra, relative intensity and structure changes of spectra are simulated as a direct consequence of the first-order anharmonic correction with respect to harmonic Franck−Condon simulation.

The understanding of anharmonic effect on spectra from analytical formulation is of importance in which it not only gives direct insight into phenomena occurring in spectra but also

† Part of the "Vincenzo Aquilanti Festschrift".

* To whom correspondence should be addressed. E-mail: cyzhu@mail.nctu.edu.tw or jianguo_yu@bnu.edu.cn.

‡ National Chiao-Tung University.

§ Beijing Normal University.

10.1021/jp903585c
Published on Web 07/01/2009

provides a way to clearly classify static with dynamic contributions to spectra in which the conventional numerical method is hard to distinguish various effects in spectra. As theoretical calculations for adiabatic potential energy differences between excited-stated and ground-state equilibrium geometries seems much larger than experimental observation of 0→0 excitation energy, we demonstrate in this paper that the discrepancy between theoretical simulations and experimental observation is actually due to the first-order anharmonic correction for the S_1 absorption and fluorescence spectra of pyridine. The certain surviving structures observed in the broaden band S_2 absorption spectrum also show up within the first-order anharmonic correction.

In Section II, we briefly introduce ab initio methods for calculation of electronic structures and normal-mode frequencies of ground and two low-lying singlet excited states of pyridine. The displaced harmonic approximation with including the first-order anharmonic correction is also discussed for Franck−Condon factors. In Section III, the simulation results of electronic structures and absorption and fluorescence spectra are reported along with comparison to experimental observations as well as some other theoretical simulations. Concluding remarks are given in Section IV.

II. Ab Initio Methods and Anharmonic Franck−Condon Factors

A. Ab Initio Methods. Both Gaussian03[49] and Molcas 7.2[50] program packages are used for the electronic structure calculations for ground state ($S_0(^1A_1)$)and the first two low-lying singlet excited states ($S_1(^1B_1)$ and $S_2(^1B_2)$). Ab initio quantum chemistry methods such as HF, CIS, CASSCF, MP2, and B3LYP methods are selected for computing the equilibrium geometries and 27 vibrational normal-mode harmonic frequencies for these three electronic states. Base sets 6-311++G** and aug-cc-pVDZ are adopted in cooperation with the methods mentioned above. We mainly report calculation results with the CASSCF method in the text because the CASSCF method is especially good for geometry optimization of aromatic molecular where resonance structures are essential. It should be mentioned that the CASSCF method does not accumulate large fractions of correlation energy, and thus it is very necessary to do the MP2 or CASPT2 correction for both excitation energy and vibrational normal-mode frequency at CASSCF geometry. The results from the other methods are given in the in Supporting Information. However, the anharmonic constants can be only computed for the ground state with B3LYP and MP2 methods using Gaussian03.

B. Anharmonic Franck−Condon Factors. The perturbation method based on harmonic oscillator as the zero-order wave function can show a clear distinction how the first-order and second-order terms contribute to molecular absorption and fluorescence spectra. Starting with perturbation expansion of the jth vibrational normal-mode potential as

$$V_j(Q) = a_{j2}Q_j^2 + \lambda a_{j3}Q_j^3 + \lambda^2 a_{j4}Q_j^4 + \cdots \qquad (2.1)$$

in which λ is chosen as a perturbation parameter and Q_j is mass-weighted normal-mode coordinate. The energy level and wave function for vibrational normal mode v_j can be expanded as a power series,

$$\varepsilon_{v_j} = \varepsilon_{v_j}^{(0)} + \lambda\varepsilon_{v_j}^{(1)} + \lambda^2\varepsilon_{v_j}^{(2)} + \cdots \qquad (2.2)$$

and

$$\chi_{v_j}(Q_j) = \chi_{v_j}^{(0)}(Q_j) + \lambda\chi_{v_j}^{(1)}(Q_j) + \lambda^2\chi_{v_j}^{(2)}(Q_j) + \cdots \qquad (2.3)$$

where $\chi_{v_j}^{(0)}(Q_j)$ denotes the harmonic wave function. Following Appendix A of ref 35, we obtain the energy level up to the second-order as

$$\varepsilon_{v_j}^{(0)} = \hbar\omega_j\left(\nu_j + \frac{1}{2}\right) \qquad (2.4)$$

$$\varepsilon_{v_j}^{(1)} = 0 \qquad (2.5)$$

and

$$\varepsilon_{\nu_j}^{(2)} = \hbar\chi_{jj}^0 + \hbar\chi_{jj}\left(\nu_j + \frac{1}{2}\right)^2 \qquad (2.6)$$

in which

$$\hbar\chi_{jj}^0 = \frac{3}{2}a_{j4}\left(\frac{\hbar}{2\omega_j}\right)^2 - \frac{7a_{j3}^2}{2\hbar\omega_j}\left(\frac{\hbar}{2\omega_j}\right)^3 \qquad (2.7)$$

and

$$\hbar\chi_{jj} = 6a_{j4}\left(\frac{\hbar}{2\omega_j}\right)^2 - \frac{30a_{j3}^2}{\hbar\omega_j}\left(\frac{\hbar}{2\omega_j}\right)^3 \qquad (2.8)$$

where χ_{jj}^0 and χ_{jj} represent the certain anharmonic constants that are estimated from the diagonal parts of the general form derived from the third and the fourth derivatives with respect normal-mode coordinates.[47,48] The wave function for the first-order correction is

$$\begin{aligned}\chi_{v_j}^{(1)}(Q_j) = -\frac{a_{j3}}{\hbar\omega_j}\left(\frac{\hbar}{2\omega_j}\right)^{3/2}\{3[\sqrt{(\nu_j+1)^3}\chi_{v_j+1}^{(0)}(Q_j) - \\ \sqrt{\nu_j^3}\chi_{v_j-1}^{(0)}(Q_j)] \\ +\frac{1}{3}[\sqrt{(v_j+1)(v_j+2)(v_j+3)}\chi_{v_j+3}^{(0)}(Q_j) - \\ \sqrt{v_j(v_j-1)(v_j-2)}\chi_{v_j-3}^{(0)}(Q_j)]\end{aligned} \qquad (2.9)$$

The first-order correction is zero for energy but is nonzero for wave function. Within the displaced anharmonic oscillator approximation of the first-order correction to harmonic oscillator, absorption coefficient is analytically derived as,[35]

$$\begin{aligned}\alpha(\omega) = \frac{2\pi\omega}{3\hbar}|\vec{\mu}_{ba}|^2\int_{-\infty}^{\infty}dt e^{it(\omega_{ba}+\Omega_0-\omega)-\gamma_{ba}|t|} \\ \times\exp[-\sum_j S_j(1+3\eta_j)\{2\bar{v}_j + 1 - (\bar{v}_j+1)e^{it\omega_j} - \\ \bar{v}_j e^{-it\omega_j}\}]\end{aligned} \qquad (2.10)$$

for excitation from electronic ground state a to excited state b that means $\omega_{ba} > 0$ in eq 2.10 for adiabatic energy gap between b and a. Fluorescence coefficient is analytically derived as well[35]

$$I(\omega) = \frac{2\pi\omega}{3\hbar}|\vec{\mu}_{ba}|^2 \int_{-\infty}^{\infty} \mathrm{dt}\, \mathrm{e}^{-it(|\omega_{ba}|+\Omega_0-\omega)-\gamma_{ba}|t|} \times \exp[-\sum_j S_j(1-3\eta_j)\{2\bar{v}_j + 1 - (\bar{v}_j+1)e^{it\omega_j} - \bar{v}_j e^{-it\omega_j}\}] \tag{2.11}$$

for excitation from electronic excited state a to ground state b that means $\omega_{ba} < 0$ in eq 2.11 for adiabatic energy gap between b and a. Other quantities are same for both eqs 2.10 and (2.11) where $\bar{v}_j = (e^{\hbar\omega_j/k_BT} - 1)^{-1}$ is the average phonon distribution, γ_{ba} represents the dephasing constant (with relation to the lifetime $\tau_{ba} = 1/\gamma_{ba}$) between two electronic states, and $\vec{\mu}_{ba}$ is the electronic transition dipole moment. The most important quantities Ω_0 and η_j stand for the first-order anharmonic correction to Fracnk-Condon factors and given by

$$\Omega_0 = -2\sum_j \eta_j S_j \omega_j \tag{2.12}$$

and

$$\eta_j = \frac{a_{j3}d_j}{a_{j2}} = \frac{a_{j3}d_j}{0.5\omega_j^2} \tag{2.13}$$

where ω_j is harmonic vabrational normal-mode frequency, and the Huang−Rhys factor S_j and the displacement d_i are defined as

$$S_j = \frac{1}{2\hbar}\omega_j d_j^2 \tag{2.14}$$

and

$$d_j = Q'_j - Q_j = \sum_n L_{jn}(q'_n - q_n) \tag{2.15}$$

where q'_n and q_n are the mass-weighted Cartesian coordinates at the equilibrium geometries of the electronic excited state and ground state, respectively. Transformation matrix **L** in eq 2.15, along with q'_n and q_n are calculated using Gaussian03 program package. If the dimensionless first-order anharmonic parameter η_j is equal to zero, the absorption coefficient in eq 2.10 and fluorescence coefficient in eq 2.11 are exactly same as displaced harmonic oscillator approximation. From the anharmonic constants in eqs 2.7 and 2.8, we can derive the following expression,

$$\eta_j^2 = -\frac{4\chi_{jj}}{\omega_j}S_j\left(1 + \frac{\chi_{jj}^0}{-\chi_{jj}/4}\right) \approx -\frac{4\chi_{jj}}{\omega_j}S_j\left(1 + \frac{\chi_0}{-\sum_j(\chi_{jj}/4)}\right) \tag{2.16}$$

where $\chi_0 = \sum_j \chi_{jj}^0$ and χ_{jj} can be calculated from Gaussian03 program package, and we assume that the ratio for each mode χ_{jj}^0/χ_{jj} is approximately equal to average ratio of summation of all modes $\sum_j \chi_{jj}^0/\sum_j \chi_{jj}$ in the second equality of eq 2.16. A sign of η_j in eq 2.16 is determined by eqs 2.15 and 2.13 where the diagonal element a_{j3} of third derivative with respect to normal-mode coordinate is estimated from Gaussian03 program package as well.

The breaking down of mirror image between absorption and fluorescence spectra is immediate consequence from the first-order anharmonic correction to Franck−Condon factors, in which the certain effective Huang−Rhys factor $S'_j = S_j(1 \pm 3\eta_j)$ (+ for absorption in eq 2.10 and − for fluorescence emission in eq 2.11) is no longer the same. The profiles of absorption and fluorescence spectra now can be very different in shape as well as in intensity.[35] Another anharmonic effect from the first-order contribution is that the harmonic 0→0 excitation energy is shifted by Ω_0 that is interpreted as a dynamic correction to the main peak of 0→0 transition in spectra. Let us discuss a possible contribution to Franck−Condon factors from the second-order anharmnoic correction before going to the next section, general form of up to the second order corrections for energy[47]

$$E = \hbar\chi_0 + \hbar\sum_j \omega_j\left(v_j + \frac{1}{2}\right) + \hbar\sum_{I<j}\chi_{ij}\left(v_i + \frac{1}{2}\right)\left(v_j + \frac{1}{2}\right) \tag{2.17}$$

in which the off-diagonal element χ_{ij} must contribute to Franck−Condon factors as the second-order anharmonic correction if we include the second-order wave function in formulating absorption coefficient in eq 2.1 and fluorescence coefficient in eq 2.11. The pairwise normal-mode mixings in the third term of eq 2.17 create the other mode-mixing that differs from the mode-mixing due to Duschinsky effect. We can distinguish Duschinsky effect as static mode-mixing with off-diagonal χ_{ij} in eq 2.17 as dynamic mode-mixing. The second-order anharmonic correction to Franck−Condon factors is our future investigation. In the present work, we concentrate on the first-order correction with application to pyridine molecule.

III. Computational Results

A. Equilibrium Geometries of S_0, S_1, and S_2 states. To accurately calculate the displacement that is difference between ground-state and excited-state geometries for simulation of absorption and fluorescence spectra, we need to optimize the equilibrium geometries of three electronic states (ground state $S_0(^1A_1)$, first excited state $S_1(^1B_1)$ and second excited state $S_2(^1B_2)$) in the equal footing. We adopt complete active space self-consistent field (CASSCF) method with consideration that pyridine consists of eight active electrons and seven active orbitals including 4 doubly occupied orbitals and 3 virtual orbitals. This selection was fully analyzed and its validity was verified.[40,41] Thus, the equilibrium geometries are optimized with high precision at the level of CASSCF(8,7)/6-311++G** and CASSCF(8,7)/aug-cc-pvDZ using both Gaussian03 and Molcas 7.2 packages, and both packages give basically the same results. All 27 normal-mode frequencies for three electronic states are computed to verify the optimized geometries as true minima of their corresponding potential energy surfaces. Table 1 shows geometry parameters (bond lengths and bond angles) of three electronic states $S_0(^1A_1)$,$S_1(^1B_1)$ and $S_2(^1B_2)$ in comparison with the experimental and the other theoretical calculations.

The measurement from electron diffraction and microwave spectroscopy[51] predicted that the ground state of pyridine molecule has a planar structure and belongs to the C_{2v} point

TABLE 1: Key Equilibrium Geometries of Ground State ($S_0(^1A_1)$), the First Excited State ($S_1(^1B_1)$) and the Second Excited State ($S_2(^1B_2)$) in Experiment, the Present and the Other Theoretical Calculations (Bond Length in Å, Angles and Dihedral Angles in deg)

method	sym	N11−C2	C2−C4	C4−C5	C1−N11−C2	N11−C2−C4	C2−C4−C5	C4−C5−C3
$S_0(^1A_1)$								
Expt[a]	C_{2v}	1.338	1.394	1.392	117	124	120	118
RHF/6-31 g*[b]	C_{2v}	1.321	1.385	1.384	118	119	117	121
B3LYP/6-311 g**	C_s	1.340	1.398	1.396	117	124	118	119
CAS(8,7)/6-311++g**	C_{2v}	1.336	1.399	1.397	118	124	119	118
CAS(6,5)/6-311 g**[c]	C_{2v}	1.320	1.384	1.383	118	123	118	119
CCSD[d]	C_{2v}	1.346	1.405	1.403	116	124	118	118
CAS(8,7)/6-31 g**[e]	C_{2v}	1.333	1.395	1.393	118	123	119	118
$S_1(^1B_1)$								
CAS(8,7)/6-311++g**	C_{2v}	1.373	1.371	1.441	129	116	120	119
CAS(6,5)/6-311 g**[c]	C_{2v}	1.368	1.351	1.432	128	116	120	119
eom-CCSD[d]	C_{2v}	1.369	1.387	1.434	129	115	121	119
$S_2(^1B_2)$								
CAS(8,7)/6-311++g**	C_{2v}	1.372	1.436	1.435	116	124	120	116
CAS(6,6)/6-311 g**[c]	C_{2v}	1.369	1.433	1.433	116	124	120	116
CAS(8,7)/6-31 g**[e]	C_{2v}	1.370	1.433	1.434	116	124	120	116
eom-CCSD[d]	C_{2v}	1.380	1.438	1.437	113	126	120	115

[a] Reference 55. [b] Reference 52. [c] Reference 40. [d] Reference 41. [e] Reference 42.

group. Table 1 shows that the present calculations agree with the experiment observation and the other theoretical simulations.[40−45] The Hartree−Fock method that does not include correlation energy shows a little bit large discrepancy with experiment and the other methods basically agree well with experiment except that B3LYP gives C_s symmetry. The detailed results with various theoretical methods for the optimized geometries are discussed in the Supporting Information.

The geometry of the first excited state is optimized by the CIS and CASSCF methods with 6-311++g** basis set, and CIS's result is not satisfactory as reported in the literatures. We report CASSCF's results in Table 1 in comparison with other theoretical calculations. The present calculation does give the same result as the others for bond lengths and bond angles within C_{2v} symmetry. Furthermore, the present CASSCF(8,7) calculations agree well with the Roos'[43] calculations with biggest active space and most active orbitals. It can also be analyzed from CASSCF calculations that the first excited state is a $^1B_1$ symmetry showing a excitation from orbital of symmetry A_1 to B_1, corresponding to a $n\rightarrow\pi^*$ transition, which confirms the calculations from the literatures. For the transition from orbital located mostly at the N atom to the anti-π orbital which has node structures between atom C4, C5 and N11, C2 in the first excited state. The angle of C1−N11−C2 rises by 10°, and bond lengths of C4−C5 and N11−C2 rise by c.a. 0.03 Å in comparison with their counterparts in ground state (numbering of atoms given in Figure 1).

The geometry of the second excited state is optimized with only CASSCF method in the 6-311++g** basis set; the present optimization shows that S_2 state also has a planar geometry of C_{2v} symmetry as in the previous theoretical calculations.[40−42] The bond lengths and angles in the present CASSCF(8,7) calculation agree with the previous theoretical calculations well. It can also be analyzed from CASSCF calculations that the second excited state is a $^1B_2$ symmetry showing a excitation from orbital of symmetry A_1 to B_1, corresponding to $\pi\rightarrow\pi^*$ transition, which is consistent with the literature. For the transition from π orbital delocalized in the plane to the anti-π orbital delocalized in the plane, all bond lengths rise by nearly 0.04 Å, while bond angles do not change much in comparison with the ground state geometry.

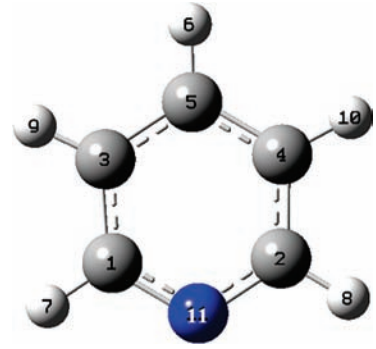

Figure 1. Atom numbering for pyridine.

B. Normal-Mode Frequencies and Anharmonic Constants. We calculate 27-normal-mode harmonic frequencies for the three electronic states $S_0(^1A_1)$,$S_1(^1B_1)$ and $S_2(^1B_2)$ using the MP2 and CASSCF methods, and we compute the corresponding anharmonic constants only for ground state $S_0(^1A_1)$ using MP2 and B3LYP methods. We list the result only for ten total symmetry A_1 modes in Table 2. Full results for all 27 vibrational normal modes are given in the Supporting Information.

We confirm all of the 27 harmonic frequencies that are positive values, so that the geometries for all three electronic states stand for the true minima of their corresponding potential energy surfaces. In comparison with measured normal-mode frequencies for ground state, both MP2 and CASSCF methods show good agreement although the MP2 method is better than the CASSCF method. The frequency difference for each normal mode between the excited states ($S_1(^1B_1)$ and $S_2(^1B_2)$) and the ground state ($S_0(^1A_1)$) is small, as shown in Table 2. This guarantees that the displaced oscillator approximation can be applied to simulate spectroscopy. The Huang−Rhys factors defined in eq 2.14 are estimated for the first and second excited states, respectively as shown in Table 2. Among 10 total symmetry normal modes, five modes υ_{6a}, υ_1, υ_{12}, υ_{13}, and υ_2 contribute to spectra significantly for the first excited state and four modes υ_{6a}, υ_1, υ_{12}, and υ_2 for the second excited state. CASSCF and MP2 give satisfactory predictions for the most contributing modes in our spectrum simulation. By following the conventional scheme for the assignment of the vibration modes,[53] we find that there are the following typical vibration

TABLE 2: Experimental (exp) and Calculated (mp2, cas/s0) Vibrational Frequencies in (cm^{-1}) for Ground State, and the Calculated Frequency Differences between $S_1(^1B_1)$ and $S_0(^1A_1)$ States (s1 − s0), and between $S_2(^1B_2)$ and $S_0(^1A_1)$ States (s2 − s0)[a]

vibration normal modes with A_1 symmetry[b]		$S_0(^1A_1)$[c]					$S_1(^1B_1)$[c]			$S_2(^1B_2)$[c]		
		exp	mp2	cas/s0	χ_{ii}	third-d	|s1 − s0|	S(s1)	d(s1)	|s2 − s0|	S(s2)	d(s2)
6a	CP	601	604	645	−0.446	4	53	1.408	0.270	83	0.116	−0.078
1	CC	991	1007	1051	−0.601	−71	101	0.495	0.131	81	1.144	0.200
12	CP	1032	1043	1103	−0.522	65	121	0.541	0.168	126	0.114	0.077
18a	HP	1072	1091	1148	−0.608	−30	58	0.002	0.014	60	0.001	0.012
9a	HP	1218	1245	1308	−0.532	32	64	0.037	−0.072	38	0.007	−0.031
19a	CC	1483	1506	1618	−3.894	−17	96	0.074	−0.077	77	0.000	0.005
8a	CC	1584	1628	1722	−6.144[d]	127	65	0.024	0.028	65	0.009	0.017
20a	CH	3030	3198	3318	−24.37[e]	−1129	20	0.077	−0.072	25	0.038	−0.051
13	CH	3074	3212	3330	−29.95[e]	861	39	0.383	0.159	28	0.004	−0.017
2	CH	3094	3237	3353	−19.22[e]	−1069[d]	45	0.120	0.088	25	0.219	0.120

[a] Calculated Huang-Rhys factors (S(s1) and S(s2)) and displacements (d(s1) and d(s2), in angstrom) for $S_1(^1B_1)$ and $S_2(^1B_2)$ states. Diagonal elements of anharmonic constants (χ_{jj} in cm^{-1}) and their corresponding third derivatives (3rd-d) for $S_0(^1A_1)$ state. [b] Mode nomenclatures from ref 53 and mode classifications from ref 51. [c] With basis set 6-311++G** in theoretical calculations. [d] MP2 calculation at single point of CASSCF optimized geometry. [e] Corresponding experiment values are about 60 cm^{-1} cited from ref 54.

TABLE 3: Calculated and Observed Vertical Excitation Energies (in eV) for $^1B_1$ and $^1B_2$ Transitions, and Its Discrepancies Δ between Theory and Experiment with Oscillator Strengths *f*

method	$^1B_1$	Δ(1)	*f*(1)	$^1B_2$	Δ(2)	*f*(2)
exp	4.59/4.45/4.74		0.003	4.99		0.029
Exp(ZPE corrected)[a]	4.75/4.61/4.90			5.13		
CASSCF(8,11)/aug-cc-pvdz[b]	5.68	0.78		5.2	0.07	
CASPT2[b]	4.93	0.03		4.88	−0.25	
CASPT2[c]	4.91	0.01	0.02	4.94	−0.19	0.04
CASPT2[d]	4.91	0.01	0.009	4.84	−0.29	0.018
SAC−CI[d]	4.59	−0.31	0.0054	4.85	−0.28	0.04
CCSD(T)[e]	4.8	−0.1	0.01	4.81	−0.32	0.03
STEOM-CCSD[f]	4.91	0.01		4.82	−0.31	
TD-B3LYP[g]	4.76	−0.14		5.47	0.34	
TD-B3LYP[b]	4.83	−0.07		5.58	0.45	

[a] Zero point corrected experimental vertical excitation energies. [b] Reference 41. [c] Reference 56. [d] Reference 57. [e] Reference 58. [f] Reference 59. [g] Reference 60.

TABLE 4: Calculated and Observed Adiabatic Excitation Energies (E_{ad}, in eV) for S_1 and S_2 States, and Its Discrepancies Δ between Theory and Experiment

method	$E_{ad}(S_1)$	Δ(1)	$E_{ad}(S_2)$	Δ(2)
Exp	4.31		4.76	
CASSCF(8,7)/aug-cc-pVDZ	4.65	0.34	4.89	0.13
CASPT2/aug-cc-pVDZ	4.57	0.26	4.73	−0.03
CASPT2/aug-cc-pVDZ[a]	4.41	0.1	4.67	−0.09
EOM-CCSD/aug-cc-pVDZ[a]	4.68	0.37	5	0.24
CAS(8,7)/6-31G**[b]	4.56	0.25	4.76	0
CASPT2/aug-cc-pVDZ[a]	4.43	0.12	4.57	−0.19
TD-B3LYP[a]	4.4	0.09	5.41	0.65

[a] Reference 41. [b] Reference 42.

modes as CC carbon−carbon stretching, CH carbon−hydrogen stretching, CP in-plane ring bend, CO out of plane ring bend, HP in-plane CH bending, and HO out of plane CH bending. Their corresponding modes are shown in Table 2. For example, the A_1 symmetry mode for $S_1(^1B_1)$ excited state (Huang−Rhys factor 1.408) corresponds to the vibration mode of 645 cm^{-1} in the CASSCF method, which could be assigned as υ_{6a} mode, namely a C−C stretching mode (CC).

Both anharmonic constants of the diagonal elements (χ_{jj} in eq 2.16) and the third-order diagonal derivative (a_{j3} in eq 2.13) with respect to normal mode coordinates are shown in Table 2, and anharmonic constants are actually not large but they can produce remarkable contribution to the spectra. We will see this later. The signs of η_j appeared in eq 2.16 are determined by d_j multiplying a_{j3}. Finally, we obtain all necessary quantities for simulating absorption spectrum with eq 2.10 and fluorescence spectrum with eq 2.11.

C. Excitation Energies. We show both the vertical and adiabatic excitation energies in Tables 3 and 4, respectively. Vertical excitation energies from calculation can be either larger or smaller than the experimental measurement varying from ab initio methods, while the adiabatic excitation energies are larger than the experimental one for the $S_1(^1B_1)$ state. Do discrepancies between experiment and calculated results totally come from accuracy problem of electronic structure calculations? Is there any dynamic effect that is not included in static property of electronic structures? Especially, the adiabatic excitation energy ω_{ab} appeared in eqs 2.10 and 2.11 comes from purely electronic structure calculation, whereas $\omega_{ab} + \Omega_{ab}$ that includes Ω_{ab} as a dynamic effect should correspond to experiment-observed excitation energy. The present work shows that this dynamic effect comes from anharmonic contribution.

For the vertical excitation from ground state to the first excited state, experiment spectrum predicted $n\rightarrow\pi^*$ transition appeared as a shoulder to the $\pi\rightarrow\pi^*$ transition which is the vertical transition from ground state to the second excited state. Therefore, the assignments of the $n\rightarrow\pi^*$ transition become controversial. Villa et al.[36] assigned that the $n\rightarrow\pi^*$ transition is located at 4.44 eV, while Goodman et al.[55] assigned it at 4.59 eV. Cai and Reimers[41] considered fluorescence excitation spectrum provided a realistic model of $^1B_1$ absorption spectrum. They extrapolated the observed fluorescence to zero signal and estimated the vertical excitation energy for $^1B_1$ to be 4.74 eV. The theoretical methods cited in Table 3 basically estimated a good agreement with experiment result except that the CASSCF gets 5.68 eV, which is too large.

For the vertical excitation from ground state to the second excited state, the experiment showed an allowed $\pi\rightarrow\pi^*$ transition, the peaks of which band maximum is located at 4.99 eV[39] with the zero-point energy correction up to 5.13 eV. As can be seen from Table 3, the TDDFT method tends to have higher excitation energies than experiment one with the values of 5.47 eV and 5.58 eV, respectively. The CASSCF method shows the best agreement with experiment one, and the other theoretical methods CASPT2, CCSD and SAC−CI estimated the vertical excitation energies lower than experiment one.

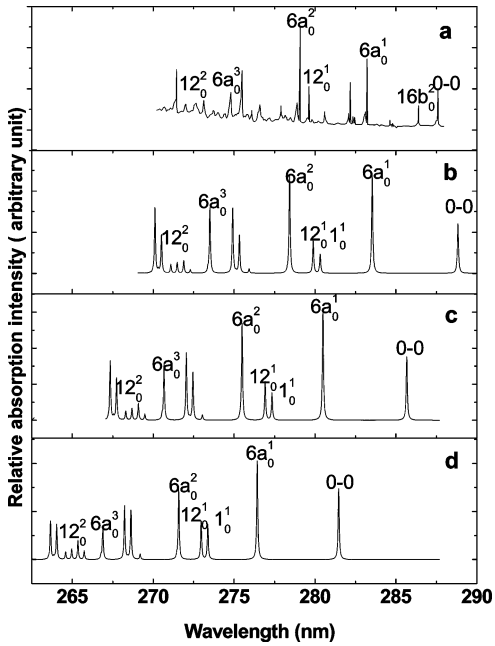

Figure 2. $S_1(^1B_1)\leftarrow S_0(^1A_1)$ absorption spectrum of pyridine and the simulation with eq 2.10. (a) Experimental data from ref 36. Spectrum simulated from the present anharmonic correction with (b) $\sqrt{3}\bar{\eta}_i$ and (c) η_i for all 10 totalsymmetry modes. (d) Spectrum simulated from the present harmonic oscillator approximation.

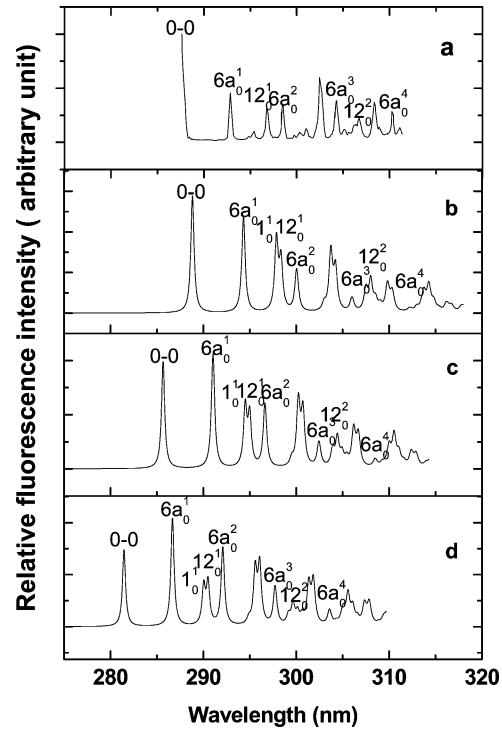

Figure 3. $S_1(^1B_1)\leftarrow S_0(^1A_1)$ fluorescence spectrum of pyridine and the simulation with eq 2.11. (a) Experimental data from ref 38. Spectrum simulated from the present anharmonic correction with (b) $\sqrt{3}\bar{\eta}_i$ and (c) η_i for all 10 total symmetry modes. (d) Spectrum simulated from the present harmonic oscillator approximation.

Regarding to oscillator strengths of the excitation, the SAC−CI[57] method obtained good results in accordance with experiment, but the CASPT2 calculations[43,56] get one order wrong. In experimental observations, the oscillator strength of $n\rightarrow\pi^*$ transition is approximately ten times smaller than that of $\pi\rightarrow\pi^*$ transition. Thus, it leads to fact in which $^1B_1$ band intensity is much smaller than $^1B_2$, and this results in that spectra of $^1B_1$ rises as the shoulder of $^1B_2$ spectrum.

Table 4 shows the adiabatic excitation energies from the ground state (S_0) to the first excited state (S_1) and to the second excited state (S_2), respectively. We utilize CASSCF(8,7)/ aug-cc-pVDZ method to obtain adiabatic excitation energies as 4.65/ 4.89 eV between S_1 /S_2 and S_0 states with CASPT2 correction down to the 4.57/4.73 eV. Actually, the present CASPT2 results are very similar to the results obtained by Becucci et al. {42} CASSCF(8,7)/ 6-31G** without the CASPT2 correction. As it can be seen in Table 4, Cai and Reimers[41] tried numerous methods and different initial geometries to predict the adiabatic excitation energies, and among their calculations the best one is that adiabatic excitation energy is 4.41/ 4.67 eV for the first/ second excited states in comparison with the experiment observation. We adopt the above adiabatic excitation energies in simulation of spectra. Although the adiabatic excitation energy is one of main parameters used in spectrum simulations, the value of the band origin only reflects on the position shift of the whole spectrum. However, we need the best static energies from the calculations in order to predict accurate dynamic correction to 0 −0 transition due to the anharmonic effect.

D. Absorption Spectra. We simulate the absorption spectra for both $S_1(^1B_1)$ and $S_2(^1B_2)$ states as shown in Figures 2 and 4, respectively, and the fluorescence emission spectrum for $S_1(^1B_1)$ state as shown in Figure 3 within both displaced harmonic and displaced anharmonic oscillator approximations. The temperature is taken as 298 K in the simulations as the experimental spectra were obtained at room temperature. The present CASSCF frequencies in Table 2 are utilized in both absorption and fluorescence spectrum simulations for the two excited states. The present dephasing constant γ_{ba} in eqs 2.10 and 2.11 are chosen as 25 and 600 cm^{-1} for the excited states $S_1(^1B_1)$ and $S_2(^1B_2)$, respectively, which are similar to that of ref 40.

The main progressions of vibrational bands for the S_1 absorption and fluorescence spectra come from υ_{6a} mode accompanied by subcontributions from modes υ_1 and υ_{12}. The Huang−Rhys factors for the modes υ_{6a}, υ_1, and υ_{12} are 1.41, 0.5, and 0.54 (see Table 2), respectively, which produce the main contribution for both absorption spectrum in Figure 2 and fluorescence spectrum in Figure 3 within the observed spectrum band region. The overall progressions of spectra are reproduced by harmonic oscillator approximation as shown in Figures 2d and 3d. In simulation of spectra with eq 2.10 for absorption and eq 2.11 for fluorescence, we utilize the best static excitation energy $|\omega_{ab}| = 4.41$ eV from Table 4 for the S_1 state, the peak position of the 0−0 excitation from harmonic oscillator approximation shows a big discrepancy with experiment observation for absorption spectrum (compare Figure 2a with d) and for fluorescence spectrum (compare Figure 3a with d). When we add anharmonic correction χ_{jj} (see Table 2) into eq 2.16 with $\chi_0/ - \sum_j(\chi_{jj}/4) \approx 2/3$ estimated from B3LYP method, we obtain anharmonic quantities η_i in eq 2.13, signs of which are determined by sign of $d_j a_{j3}$ *from Table 2*. In this way, we obtain spectrum shift $\Omega_0 = -523$ cm^{-1} in eq 2.12 in which the minus corresponds to red shift of spectrum as can be seen from Figures 2c and 3c. In fact, the anharmonic constants χ_{jj} computed from Gaussian are not accurate enough (see Table 2) in which the experiment values for the highest three vibrational-normal modes (over 3300 cm^{-1}) are two to three times bigger than computed ones. With scaling scheme that is widely used in harmonic frequency calculation, we make a factor of 3 to all anharmonic constants χ_{jj} in Table 2 so that η_i in eq 2.13 becomes $\sqrt{3}\bar{\eta}_i$, which leads to spectrum shift $\Omega_0 = -\sqrt{3}*523$ cm^{-1}. This results in the correct peak position for 0−0 transition as well as the

other peaks in spectra depicted in Figure 2b for absorption and Figure 3b for fluorescence. We conclude that $\Omega_0 = -0.11$ eV is dynamic correction to static adiabatic excitation energy $|\omega_{ab}| = 4.41$ eV. At the same time, the anharmonic quantity $\eta_{6a} = 0.08$ computed from eq 2.16 makes effective the Huang−Rhys factor for absorption as $S'_{6a} = S_{6a}(1 + 3\eta_{6a}) = 1.75$ and for fluorescence as $S'_{6a} = S_{6a}(1 - 3\eta_{6a}) = 1.1$, which leads to υ_{6a} transition profiles and relative intensity changes as well, as illustrated in Figures 2c and 3c. With factor of 3 scaling to anharmonic constants χ_{ij}, we finally simulate absorption spectrum in Figure 2b and fluorescence spectrum in Figure 3b that is in good agreement with experiment. The first-order anharmonic correction makes both spectra shift and profile change simultaneously in the right direction in comparison with experimental absorption and fluorescence spectra for S_1 state. The CASSCF frequencies are utilized in spectrum simulations and overall spectra band widths are wider than experiment ones mainly due to discrepancy of 6a-mode frequency between calculation and experiment (about 45 cm^{-1} difference).

Let us now start to analyze the S_2 absorption spectrum. The largest Huang−Rhys factor for the $S_2(^1B_2)$ state listed in Table 2 is 1.14 for vibrational mode υ_1 accompanied by the other two, 0.116 for the mode υ_{6a} and 0.118 for mode υ_{12}. The highest peak from experimental is assigned as the 1_0^2 vibronic transition, while the present calculation shows 1_0^1 as the strongest transition. The present harmonic displaced oscillator approximation simulates absorption spectrum depicted in Figure 4d in which the spectrum profile has two shoulders similar to what Cai and Reimers simulated by including the Duschinsky effects as shown in Figure 3 of ref 41. This probably means that Duschinsky effects are not important. When we add anharmonic correction, the two shoulders disappear and profile structure around peak position turns to be in accordance with experimental spectrum shape (compare Figure 4a with c). The spectrum shift is now equal to $\Omega_0 = +281$ cm^{-1} in eq 2.12 in which the plus corresponds to blue shift of spectrum as can be seen from Figure 4c. With scaling of a factor of 2 to all anhramonic constants χ_{jj} in Table 2, the spectrum shift becomes $\Omega_0 = \sqrt{2}*281$ $cm^{-1} = 0.04$ eV, which is in correct direction in comparison with experiment 0−0 transition. Similarly, spectrum shape around peak position is getting more close to experimental profile. As $\eta_1 = 0.066$ cm^{-1} for mode 1, it is still too small to make effective Huang−Rhys factor $S'_1 = S_1(1 + 3\eta_{6a}) = 1.34$ larger than 2 which is necessary for identifying 1_0^2 vibronic transition as the strongest one. Nevertheless, the present anharmonic correction make spectrum shift and profile change in the right direction in comparison with experiment observation. The harmonic displaced oscillator approximation with including distorted effect in ref 40 did not show up detail structure around peak position. We could conclude that the first-order anharmonic correction does make an important contribution to absorption spectrum for S_2 state.

IV. Concluding Remarks

We have simulated both absorption and fluorescence spectra for S_1 state and absorption spectrum for S_2 state of pyridine by using both displaced harmonic and anharmonic oscillator approximation. We found that the first-order anharmonic correction make a significant contribution to band shift and profile changes of spectra for pyridine molecule. We have utilized both CASSCF method to compute the equilibrium geometries of the electronic ground and the lowest two-singlet excited states of pyridine with their 27-normal-mode frequencies. All three electronic states show a C_{2v} symmetry, and calculation results

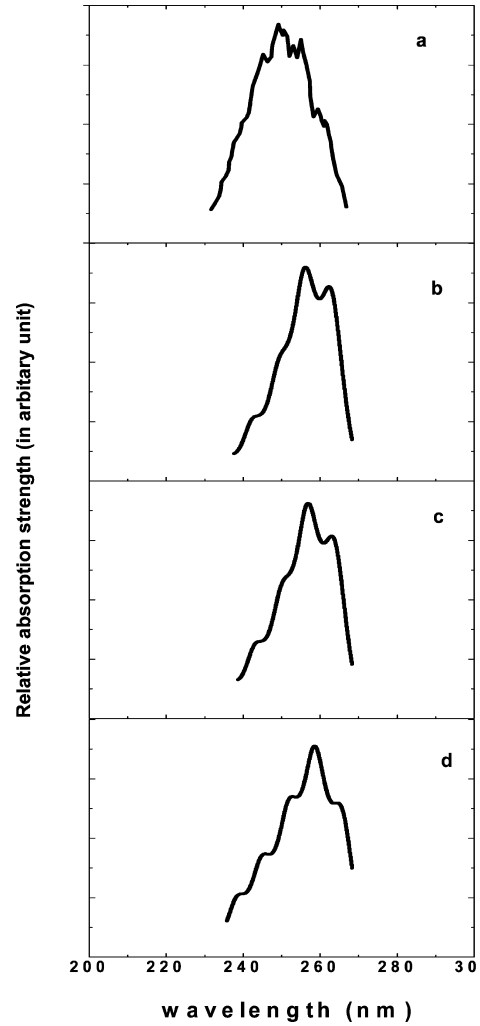

Figure 4. $S_2(^1B_2)$←$S_0(^1A_1)$ absorption spectrum of pyridine and the simulation with eq 2.10. (a) Experimental data from ref 39. Spectrum simulated from the present anharmonic correction with (b) $\sqrt{2}\bar{\eta}_i$ and (c) η_i for all 10 total symmetry modes. (d) Spectrum simulated from the present harmonic oscillator approximation.

are basically the same as those from high-level Ab. initio calculation in the literatures. This makes that the equilibrium geometries from the present calculation are accurate enough to be used for spectrum simulations.

The electronic structure calculations confirm that the $S_1(^1B_1)$ and $S_2(^1B_2)$ states have $n\pi^*$ and $\pi\pi^*$ configurations, respectively. Both cited vertical and calculated adiabatic excitation energies of the $S_1(^1B_1)$ and $S_2(^1B_2)$ states are discussed and analyzed by cross comparison with various theoretical calculations and experimental results. Basically, even the best calculations for static adiabatic excitation energies of the $S_1(^1B_{3u})$ and $S_2(^1B_{2u})$ states differ from the experimental ones. With the present anharmonic correction computed from B3LYP and MP2 methods, we could extract the excitation energies from dynamic effect so that experiment excitation energies should include both the calculated static excitation energies and dynamic shift.

The present studies indicate that, for the three electronic states of pyridine, $S_0(^1A_1)$, $S_1(^1B_1)$, and $S_2(^1B_2)$, the frequencies of the 10 total symmetric normal modes only slightly differ from one another. Furthermore, we obtain the transformation matrices that transfer system from Jacobi to normal-mode coordinates for the three electronic states, and we find that the corresponding matrices for the 10 total symmetric modes are quite similar. Thus, displaced harmonic and anharmonic oscillator approxima-

tions can be used for simulation. In fact, from Huang−Rhys factors we conclude that the modes υ_{6a}, υ_1, and υ_{12} contribute S_1 absorption and fluorescence spectra and S_2 absorption spectrum mostly, among which the main progression of S_1 bands comes from mode υ_{6a} and S_2 bands comes from mode υ_1. This agrees with experimental measurement. The present first-order anharmonic corrections can only take into account diagonal part of anharmonicity, and mode mixings (differ from Duschinsky mode mixings) due to off-diagonal part of anharmonicity are completely neglected as they belong to the second-order anharmonic corrections. The conventional Herzberg−Teller effect of intensity borrowing from the other nontotally symmetric vibrational modes and possible nonadiabatic coupling due to conical intersection are not considered in the present studies as the both have little effect to totally symmetric vibrational modes.

In conclusion, simulations of absorption and fluorescence spectra from the adiabatic $S_1(^1B_1)$ and $S_2(^1B_2)$ states show good agreement with experimental observation with taking into account the first-order anharmonic correction to harmonic Franck−Condon simulation. Anharmonic correction plays the most significant role for pyridine spectra in comparison with distorted effects or/and Duschinsky effects.

Acknowledgment. H.W. thanks support from visiting graduate program in National Chiao Tung University. This work is supported by National Science Council of the Republic of China under grant no. 97-2113-M-009-010-MY3, and by National Natural Science Foundation of People's Republic of China under grant nos. 20573011, 20733002, and 20873008 and Major State Basic Research Development Programs (Grant no. 2004CB719903). C.Z. thanks the MOE-ATU project of the National Chiao Tung University for support.

Supporting Information Available: Details of geometry optimizations, excitation energies, all 27 harmonic vibrational frequencies, and all 27 anharmonic constants, as well as absorption and fluorescence spectra contributed from individual vibrational mode are summarized with various ab initio quantum chemistry methods. This material is available free of charge via the Internet at http://pubs.acs.org.

References and Notes

(1) Franck, J. *Trans. Faraday Soc.* **1925**, *21*, 536.
(2) Condon, E. U. *Phys. Rev.* **1926**, *28*, 1182.
(3) Condon, E. U. *Phys. Rev.* **1928**, *32*, 858.
(4) Duschinsky, F. *Acta Physicocchim. URSS* **1937**, *7*, 551.
(5) Sharp, T. E.; Rosenstok, H. M. *J. Chem. Phys.* **1964**, *41*, 3453.
(6) Lin, S. H. *J. Chem. Phys.* **1966**, *44*, 3759.
(7) Lin, S. H.; Bersohn, R. *J. Chem. Phys.* **1966**, *44*, 3768.
(8) Lin, S. H. *J. Chem. Phys.* **1973**, *58*, 5760.
(9) Cederbaum, L.S.; W.; Domcke, W. *J. Chem. Phys.* **1976**, *64*, 603.
(10) Doktorov, E. V.; Malkin, I. A.; Man'ko, V. I. *J. Mol. Spectrosc.* **1977**, *64*, 302.
(11) Dewar, M. J. S.; Zoebisch, E. G.; Healy, E. F.; Stewart, J. J. P. *J. Am. Chem. Soc.* **1985**, *107*, 3902.
(12) Roche, M. *Chem. Phys. Lett.* **1990**, *168*, 556.
(13) Lee, S. *J. Phys. Chem. A* **1990**, *94*, 4420.
(14) Todd, D. C.; Fleming, G. R.; Jean, J. M. *J. Chem. Phys.* **1992**, *97*, 8915.
(15) Zerbetto, F. *J. Phys. Chem. A* **1994**, *98*, 13157.
(16) Ruhoff, P. T. *Chem. Phys.* **1994**, *186*, 355.
(17) Malmqvist, P.; Forsberg, N. *Chem. Phys. Lett.* **1998**, *228*, 227.
(18) Müller, T.; Vaccaro, P. H.; Perez-Bernal, F.; Ibrahim, M.; Iachello, F. *J. Chem. Phys.* **1999**, *111*, 5038.
(19) Mok, D. K. W.; Lee, E. P. F.; Chau, F.; Wang, D.; Dyke, J. K. *J. Chem. Phys.* **2000**, *113*, 5791.
(20) Ruhoff, P. T.; Ratner, M. A. *Int. J. Quantum Chem.* **2000**, *77*, 383.
(21) Schumm, S.; Gerhards, M.; Kleinermanns, K. *J. Phys. Chem. A* **2000**, *104*, 10648.
(22) Reimers, J. R. *J. Chem. Phys.* **2001**, *115*, 7076.
(23) Zazubovich, V.; Tibe, I.; Small, G. J. *J. Phys. Chem. B* **2001**, *105*, 12410.
(24) Lin, S. H.; Chang, C. H.; Liang, K. K. et al. *Advanced Chemical Physics*, Vol. 121; Prigogine, I., Rice, S. A., Eds.; Wiley: New York, 2002; p 1.
(25) Kikuchi, H.; Kubo, M.; Watanabe, N.; Suzuki, H. *J. Chem. Phys.* **2003**, *119*, 729.
(26) Hwang, H.; Rossky, P.; Jean, *J. Phys. Chem. A* **2004**, *108*, 2607.
(27) Luis, J. M.; Bishop, D. M.; Kirtman, B. *J. Chem. Phys.* **2004**, *120*, 813.
(28) Hazra, A.; Chang, H. H.; Nooijen, M. *J. Chem. Phys.* **2004**, *121*, 2125.
(29) Dierksen, M.; Grimme, S. *J. Phys. Chem. A* **2004**, *108*, 10225.
(30) Dierksen, M.; Grimme, S. *J. Chem. Phys.* **2005**, *122*, 244101.
(31) Yeganeh, S.; Ratner, M. A. *J. Chem. Phys.* **2006**, *124*, 044108.
(32) Pugliesi, I.; Muller, D. K. *J. Phys. Chem. A* **2006**, *110*, 4657.
(33) Pugliesi, I.; Muller, D. K. *J. Phys. Chem. A* **2006**, *110*, 13045.
(34) Hayashi, M.; Shiu, Y. J.; Liang, K. K.; Lin, S. H.; Shen, Y. R. *J. Phys. Chem. A* **2007**, *111*, 9062.
(35) Zhu, C.; Liang, K. K.; Hayashi, M.; Lin, S. H. *Chem. Phys.* **2009**, *358*, 137.
(36) Villa, E.; Amirav, A.; Lim, E. C. *J. Phys. Chem.* **1988**, *92*, 5393.
(37) Becucci, M.; Lakin, N. M.; Pietraperzia, G.; Salvi, P. R.; Castellucci, E.; Kerstel, E. R. T. *J. Chem. Phys.* **1997**, *107*, 10399.
(38) Mochizuki, Y.; Kaya, K.; Ito, M. *J. Chem. Phys.* **1978**, *69*, 935.
(39) Bolovinos, A.; Tsekeris, P.; Pantos, J.; Andritsopoulos, G. *J. Mol. Spectrosc.* **1984**, *103*, 240.
(40) Wu, D.-Y.; Hayashi, M.; Shiu, Y. J.; Liang, K. K.; Chang, C. H.; Lin, S. H. *J. Chin. Chem. Soc.* **2003**, *50*, 735.
(41) Cai, Z. L.; Reimers, J. R. *J. Phys. Chem. A* **2000**, *104*, 8389, and references therein.
(42) Becucci, M.; Lakin, N. M.; Pietraperzia, G.; Salvi, P. R.; Castellucci, E.; Kerstel, E. R. T. *J. Chem. Phys.* **1997**, *107*, 10399.
(43) Lorentzon, L.; Fulscher, M. P.; Roos, B. O. *Theor. Chim.Acta* **1995**, *92*, 67.
(44) Riese, M.; Altug, Z.; Grotemeyer, J. *Phys. Chem. Chem. Phys.* **2006**, *8*, 4441.
(45) Martin, Jan, M. L.; Van Alsenoy, C. *J. Phys. Chem.* **1996**, *100*, 6973.
(46) Kitao, O.; Nakatsuji, H. *J. Chem. Phys.* **1988**, *88*, 4913.
(47) Barone, V. *J. Chem. Phys.* **2004**, *120*, 3059.
(48) Barone, V. *J. Chem. Phys.* **2005**, *122*, 014108.
(49) Frisch, M. J.; Trucks, G. W.; Schlegel, H. B.; et al. *Gaussian*, Revision D02; Gaussian, Inc.: Wallingford CT, 2004.
(50) Karlström, G.; Lindh, R.; Malmqvist, P.-Å.; Roos, B. O.; Ryde, U.; Veryazov, V.; Widmark, P.-O.; Cossi, M.; Schimmelpfennig, B.; Neogrady, P.; Seijo, L. *Comput. Mater. Sci.* **2003**, *28*, 222.
(51) Innes, K. K.; Ross, I. G.; Moomaw, M. R. *J. Mol. Spectrosc.* **1988**, *132*, 492.
(52) Foresman, J. B.; Head-Gordon, M.; Pople, J. A.; Frisch, M. J. *J. Phys. Chem.* **1992**, *96*, 135.
(53) Lord, R. C.; Marston, A. L.; Miller, F. A. *Spectrochim. Acta* **1957**, *9*, 113.
(54) Snavely, D. L.; Overly, J. A.; Waiters, V. A. *Chem. Phys.* **1995**, *201*, 567.
(55) Goodman, L. *J. Mol. Spectrosc.* **1961**, *6*, 109.
(56) Fülscher, M. P.; Andersson, K.; Roos, B. O. *J. Phys. Chem.* **1992**, *96*, 9204.
(57) Wan, J.; Hada, M.; Ehara, M.; Nakatsuji, H. *J. Chem. Phys.* **2001**, *114*, 5117.
(58) Del-Bene, J. E.; Watts, J. D.; Bartlett, R. J. *J. Chem. Phys.* **1997**, *106*, 6051.
(59) Nooijen, M.; Bartlett, R. J. *J. Chem. Phys.* **1997**, *106*, 6441.
(60) Bauernschmitt, R.; Ahlrichs, R. *Chem. Phys. Lett.* **1996**, *256*, 454.

JP903585C